Inorg. Chem. **2007**, *46*, 10416–10425

High T_c Ferrimagnetic Organic–Inorganic Hybrid Materials with Mn^{II}–L–Mn^{II} and Mn^{II}–NC–Nb^{IV} Linkages (L = Pyrazine, Pyrazine-*N*,*N*′-dioxide, Bipyrimidine)

Robert Podgajny,*,† Dawid Pinkowicz,† Tomasz Korzeniak,† Wojciech Nitek,† Michał Rams,‡ and Barbara Sieklucka*,†

Faculty of Chemistry, Jagiellonian University, Ingardena 3, 30-060 Kraków, Poland and M. Smoluchowski Institute of Physics, Jagiellonian University, Reymonta 4, 30-059 Kraków, Poland

Received September 14, 2007

A series of heterobimetallic, cyano-bridged 3D inorganic–organic hybrid networks with Mn^{II}–L–Mn^{II} and Mn^{II}–NC–Nb^{IV} linkages are reported. Reaction of $[Mn(H_2O)_6]^{2+}$ with $[Nb(CN)_8]^{4-}$ in the presence of organic linker L (pyrazine (pyz), pyrazine-*N*,*N*′-dioxide (pzdo), and 2,2′-bipyrimidine (bpym)) in H_2O affords $\{Mn^{II}_2(pz)_2(H_2O)_4[Nb^{IV}(CN)_8]\}\cdot pz\cdot 3H_2O$ (**1**), $\{Mn^{II}_2(pzdo)(H_2O)_4[Nb^{IV}(CN)_8]\}\cdot 5H_2O$ (**2**), and $\{Mn^{II}_2(bpym)(H_2O)_2[Nb^{IV}(CN)_8]\}$ (**3**), respectively. **1**–**3** were examined by X-ray crystallography and vibrational and magnetochemical studies. **1** is characterized by the coexistence of 3D inorganic cyano-bridged and 1D organic $[Mn–(\mu\text{-pyz})]_n^{2n+}$ sublattices along with the presence of monocoordinated and crystallization molecules of pyrazine. Assemblies **2** and **3** exhibit dimeric $\{Mn^{II}_2–(\mu\text{-L})\}^{4+}$ coordination motifs. The magnetic behavior of heterobimetallic **1**–**3** complexes is dominated by antiferromagnetic coupling between Mn^{II} and Nb^{IV} centers mediated by cyano bridges, resulting in long-range ferrimagnetic ordering with a high T_C of 27 (**1**), 37 (**2**), and 50 K (**3**). The magneto-structural correlation leads to the conclusion that the magnitude of T_C is related to the type of coordination polyhedra of $[Nb(CN)_8]$ moieties (SAPR (**1**), intermediate between SAPR and DD (**2**), and DD (**3**)), the relative number of cyano bridges per Mn_2Nb unit, and coexistence of inorganic and organic connectivity. FC/ZFC responses appear to be sensitive to the degree of organic connectivity. The discussion of magneto-structural correlation is based on the spin-density properties of adequate heterobimetallic systems containing octacyanometalates.

Introduction

High-dimensional architectures of coordination compounds have received an enormous amount of attention over the last decades due to the variety of phenomena related to the magnetic interaction between metal centers through molecular bridges. The numerous magnetic assemblies were characterized by the transitions to/between the ordered (ferro, ferri, antiferro, including canted) magnetic structures with high T_c.[1−24] The particular impact was observed for the 3D cyano-bridged Prussian blue analogues, which revealed T_c ranging from liquid helium to temperatures exceeding room temperature.[1−3] The structural similarities of the Prussian blue family members allowed correlating the magnitude of T_c and type of long-range ordering in relation to the electronic configuration and spin state of the metal centers.[3a] This

* To whom correspondence should be addressed. E-mail: (R.P.) podgajny@chemia.uj.edu.pl, (B.S.) siekluck@chemia.uj.edu.pl.
† Faculty of Chemistry, Jagiellonian University.
‡ M. Smoluchowski Institute of Physics, Jagiellonian University.

(1) Ferlay, S.; Mallah, T.; Ouahès, R.; Veillet, P.; Verdaguer, M. *Nature* **1995**, *378*, 701−703.
(2) Holmes, S. M.; Girolami, G. S. *J. Am. Chem. Soc.* **1999**, *121*, 5593−5594.
(3) (a) Verdaguer, M.; Bleuzen, A.; Marvaud, V.; Vaissermann, J.; Seuleimenn, M.; Desplanches, C.; Scuiller, A.; Train, C.; Garde, R.; Gelly, G.; Lomenech, C.; Rosenman, I.; Veillet, P.; Cartier dit Moulin, C.; Villain, F. *Coord. Chem. Rev.* **1999**, *190−192*, 1023−1047. (b) Verdaguer, M.; Villain, F.; Ouahès, R.; Galvez, N.; Garde, R.; Keller, G.; Tournilhac, F. *Polyhedron* **2005**, *24*, 2906−2908.
(4) Inoue, K.; Hayamizu, T.; Iwamura, H.; Hashizume, D.; Ohashi, Y. *J. Am. Chem. Soc.* **1996**, *118*, 1803−1804.
(5) Manson, J. L.; Kmety, C. R.; Epstein, A. J.; Miller, J. S. *Inorg. Chem.* **1999**, *38*, 2552−2553.
(6) Pokhodnya, K. I.; Bonner, M.; Her, J.-H.; Stephens, P. W.; Miller, J. S. *J. Am. Chem. Soc.* **2006**, *128*, 15592−15593.
(7) Larionova, J.; Clérac, R.; Sanchiz, J.; Kahn, O.; Golhen, St.; Ouahab, L. *J. Am. Chem. Soc.* **1998**, *120*, 13088−13095.
(8) Larionova, J.; Kahn, O.; Golhen, St.; Ouahab, L.; Clérac, R. *J. Am. Chem. Soc.* **1999**, *121*, 3349−3356.
(9) Kahn, O.; Larionova, J.; Ouahab, L. *Chem. Commun.* **1999**, 945−952.

10.1021/ic7018132 CCC: $37.00
Published on Web 10/27/2007

research allowed the rational design and construction of the device using the properties of the room-temperature magnet to transform light into mechanical energy.[3b]

Functional organic−inorganic hybrid networks are extremely interesting due to properties such as magnetism, spin crossover, conductivity, porosity, luminescence, and chirality functions.[25−28] However, construction of the functional cyano-bridged network which incorporates an organic linker (i.e., carboxylate, oxalate, and heterocyclic N donors) is a challenge.[29−32] There are limited examples that involve heterobimetallic organic−inorganic hybrid networks built by octacyanometalates of Mo and W (Table 1).[31−37] Introduction of acetate, pyrazine (pz), pyrimidine (pym), 4,4′-bipyridine (4,4′-bpy), or 2,2′-bipyrimidine (2,2′-bpym) organic linker to cyano-bridged bimetallic framework resulted in 2D or 3D assemblies; some of them are characterized by relatively high T_c[31,32,34,36] along with light- and temperature-tuned magnetic response.[31]

Another member of the octacyanometalate family, paramagnetic $[Nb^{IV}(CN)_8]^{4-}$ precursor, has been very scarcely employed as a building block in formation of cyano-bridged coordination networks. The divergent $[Mn(H_2O)_6]^{2+}$ gener-

Table 1. Organic−Inorganic Hybrid Networks Built by Octacyanometalates of Mo and W

formula	structural feature (dimensionality of organic and inorganic connectivity)[a]	magnetic features	ref
$[Mn^{II}_2(H_2O)_2(CH_3CO_2)][W^V(CN)_8]\cdot 2H_2O]_n$	3D W−CN−Mn, 0D dimeric $\{Mn_2(\mu\text{-Ac})\}$	$T_C = 40$ K	32
$\{Mn^{II}_2Cs_{0.5}[W^V(CN)_8](CH_3CO_2)_{1.5}(H_2O)\}_n$	3D W−CN−Mn, 0D zigzag tetrameric $\{Mn_4(\mu\text{-Ac})_3\}$	$T_C = 45$ K	32
$\{(\mu\text{-bpym})[Mn^{II}(H_2O)]_2\text{-}\mu\text{-}(NC)_6M^{IV}(CN)_2\}_n$ (M = Mo, W)	3D M−CN−Mn, 0D dimeric $\{Mn_2(\mu\text{-bpym})\}$	$J_{Mn-bpym-Mn}$ of ~1 cm^{-1}	33
$\{[Mn^{II}(pym)(H_2O)]_2[Mn^{II}(H_2O)_2][W^V(CN)_8]_2\}_n$	3D W−CN−Mn, 0D linear dimeric $\{(pym-Mn)_2-(\mu\text{-pym})\}$, crystallization pym	$T_C = 47$ K	34
$Cs^I\{[Co^{II}(\mu\text{-pym})_2][W^V(CN)_8]\cdot H_2O$	3D W−CN−Co, 0D zigzag trimeric $\{Mn_3-(\mu\text{-pym})_2\}$, crystallization pym	CTIST: $T_{1/29} = 208$ K, $T_{1/28} = 298$ K; LIESST: $T_c = 40$ K, $H_c = 12$ T	31
$[Cs^{II}(\mu\text{-}4,4\text{-bpy})]_3[W^V(CN)_8]_2\cdot 6DMF\cdot 2H_2O$	1D 3,2 chain W−CN−Cu, 1D linear chains $\{Cu-(\mu\text{-}4,4,\text{-bpy})\}$	$J_{W-CN-Cu} = 35$ cm^{-1}	35
$\{Co^{II}_3(H_2O)_6(pz)_3[W^V(CN)_8]_2\}\cdot 3.5H_2O$	W−CN−Co, 1D $\{Co-(\mu\text{-pyz})\}^b$	$T_C = 26$ K	36
$\{Co^{II}_3(H_2O)_4(4,4\text{-bpy})_3[W^V(CN)_8]_2\}\cdot 1.5(4,4\text{-bpy})\cdot 6H_2O$	W−CN−Co, 1D $\{Co-(\mu\text{-}4,4\text{-bpy})\}^b$	$T_C = 16$ K, $T_C = 11$ K	36
$(Me_3Sn)_4[Mo(CN)_8]\cdot 0.5pyz$	hydrogen-bonded L guest ligands in high dimensional Mo−CN−SnMe3 network[c]		38

[a] Abbreviations: Ac = acetate, bpym = bipyrimidine, pym = pirymidine, 4,4′-bpy = 4,4′-bipyridine, pyz = pyrazine. [b] Not characterized by X-ray diffraction; connectivity proposed basing on IR, magnetic, and ES-MS and literature data. [c] No bridging mode of L.

(10) Sra, A. K.; Rombaut, G.; Lahitête, F.; Golhen, St.; Ouahab, L.; Mathonière, C.; Yakhmi, J. V.; Kahn, O. *New J. Chem.* **2000**, *24*, 871−876.
(11) Tanase, St.; Tuna, F.; Guionneau, Ph.; Maris, Th.; Rombaut, G.; Mathonière, C.; Andruh, M.; Kahn, O.; Sutter, J.-P. *Inorg. Chem.* **2003**, *42*, 1625−1631.
(12) Mathonière, C.; Nuttall, Ch. J.; Carling, S. G.; Day, P. *Inorg. Chem.* **1996**, *35*, 1201−1206.
(13) Armentano, D.; De Munno, G.; Mastropietro, T. F.; Proserpio, D. M.; Julve, M.; Lloret, F. *Inorg. Chem.* **2004**, *43*, 5177−5179.
(14) Zhang, Y.-Zh.; Wang, Zh.-M.; Gao, S. *Inorg. Chem.* **2006**, *45*, 5447−5454.
(15) Xu, H.-B.; Wang, Zh.-M.; Liu, T.; Gao, S. *Inorg. Chem.* **2007**, *46*, 3089−3096.
(16) Navarro, J. A. R.; Barea, E.; Salas, J. M.; Maschiocchi, N.; Galli, S.; Sironi, A. *Inorg. Chem.* **2007**, *46*, 2988−2997.
(17) Ma, B.-Q.; Sun, H.-L.; Gao, S.; Su, G. *Chem. Mater*. **2001**, *13*, 1946−1948.
(18) Zhong, Zh.-J.; Seino, H.; Mizobe, Y.; Hidai, M.; Verdaguer, M.; Ohkoshi, Sh-ich.; Hashimoto, K. *Inorg. Chem.* **2000**, *39*, 5095−5101.
(19) Podgajny, R.; Korzeniak, T.; Bałanda, M.; Wasiutyński, T.; Errington, W.; Kemp, T. J.; Alcock, N. W.; Sieklucka, B. *Chem. Commun.* **2002**, 1138−1139.
(20) Arimoto, Y.; Ohkoshi, Sh.-ich.; Zhong, Z. J.; Seino, H.; Mizobe, Y.; Hashimoto, K. *Chem. Lett.* **2002**, *8*, 832−833.
(21) Arimoto, Y.; Ohkoshi, Sh.-ich.; Zhong, Z. J.; Seino, H.; Mizobe, Y.; Hashimoto, K. *J. Am. Chem. Soc.* **2003**, *125*, 9240−9241.
(22) Podgajny, R.; Chmel, N. P.; Bałanda, M.; Tracz, P.; Gaweł, B.; Zaja<crn>c, D.; Sikora, M.; Kapusta, Cz.; Łasocha. W.; Wasiutyński, T.; Sieklucka, B. *J. Mater. Chem.* **2007**, 3308−3314.
(23) Yanai, N.; Kaneko, W.; Yoneda, K.; Ohba, M.; Kitagawa, S. *J. Am. Chem. Soc.* **2007**, *129*, 3496−3497.
(24) Withers, J. R.; Li, D.; Triplet, J.; Ruschman, Ch.; Parkin, S.; Wang, G.; Yee, G. T.; Holmes, St. *Inorg. Chem.* **2006**, *45*, 4307.
(25) Janiak, Ch. *Dalton Trans.* **2003**, 2781−2840.
(26) Kitagawa, S.; Kitaura, R.; Noro, Sh.-ich. *Angew. Chem., Int. Ed.* **2004**, *43*, 2334−2375.
(27) Cheetham, A. K.; Rao, C. N. R.; Feller, R. K. *Chem. Commun.* **2006**, 4780−4795.
(28) Maspoch, D.; Ruiz-Molina, D.; Veciana, J. *Chem. Soc. Rev.* **2007**, *36*, 770−818.
(29) Bonhommeau, S.; Molnár, G.; Galet, A.; Zwick, A.; Real, J.-A.; McGarvey, J. J.; Bousseksou, A. *Angew. Chem., Int. Ed.* **2005**, *44*, 4069−4073.
(30) Molnár, G.; Niel, V.; Real, J.-A.; Dubrovinski, L.; Bousseksou, A.; McGarvey, J. J. *J. Phys. Rev. B* **2003**, *107*, 3149−3155.
(31) Ohkoshi, Sh.-ich.; Ikeda, S.; Hozumi, T.; Kashigawi, T.; Hashimoto, K. *J. Am. Chem. Soc.* **2006**, *128*, 5320−5321.
(32) Song, Y.; Ohkoshi, Sh.-ich.; Arimoto, Y.; Seino, H.; Mizobe, Y.; Hashimoto, K.; *Inorg. Chem.* **2003**, *42*, 1848−1856.

ated 3D $\{Mn^{II}_2(H_2O)_4[Nb^{IV}(CN)_8]\cdot 4H_2O\}$ consisting of mutually perpendicular 2D Mn_2Nb square-grid sheets cross-linking in Nb centers, characterized by a transition to the ferrimagnetic phase at $T_C = 50$ K.[38] Each $[Nb(CN)_8]^{4-}$ moiety coordinates eight Mn^{II} centers, while Mn^{II} is bridged to four octacyanoniobates(IV), giving rise to Nb:Mn = 8:4 inorganic connectivity. Use of *trans*-$\{MnL^1(H_2O)_2\}^{2+}$ and *trans*-$\{NiL^2(H_2O)_2\}^{2+}$ complexes, where L^1 and L^2 are four- and five-coordinative macrocyclic ligands, respectively, afforded 1D $\{[MnL^1]_2[Nb(CN)_8](H_2O)\cdot 5H_2O\}_\infty$ and discrete $\{[NiL^2]_{12}[Nb(CN)_8]_6(H_2O)_6\}\cdot 100H_2O$ assemblies.[39] Both compounds are characterized by the alternative 1:1 arrangement of the 3d metal and niobium(IV) moieties, chain-like in the former and ring-like in the latter, with the additional $[ML(NC)(H_2O)]^+$ moiety pending out of the basic coordination unit. Antiferromagnetic interaction between 3d metal and niobium centers through cyano bridges was observed for both assemblies.

Several theoretical approaches were applied to explain the origin of the effective intermetallic magnetic coupling or/and long-range ordering in 3D 3d-metals−octacyanometalates assemblies.[32,34,40−43] The critical factor modulating the magnetism in these systems is a type of coordination polyhedra of participating metal centers influencing the electronic ground state as well as the spin density transferred onto the molecular orbitals of cyano bridges. It was shown that highly symmetrical SAPR $[Mo(CN)_8]^{3-}$ and $[W(CN)_8]^{3-}$ ions (d_{z2}^1 ground state) are characterized by an almost identical spin density distribution over all eight cyano bridges, while the lower symmetry DD ions (d_{x2-y2}^1 ground state) reveal significantly increased spin density for privileged equatorial positions B and decreased spin density for the apical positions A compared to those of SAPR.[41,42] This difference is well illustrated in the case of the Mn(II)−Mo(V) antiferromagnetic interactions considered for dinuclear Mn−NC−Mo linkages extracted from Mo_6Mn_9 high-spin cluster, where the $|J|$ value for CN^- bridges at position B were significantly higher compared to those of position A.[41] Another crucial factor is the type of coordination polyhedra of the 3d metal center. It has been shown that 3D $Mn^{II}_2[Mo^{III}(CN)_7]$ networks reveal long-range ordering of T_C increasing with decreasing coordination number (C.N.) and change of coordination polyhedra: for *cis*-$[Mn^{II}(\mu\text{-}NC)_4(H_2O)_2]$ (C.N. = 6) and *mer*-$[Mn^{II}(\mu\text{-}NC)_3(H_2O)_3]$ (C.N. = 6) $T_C = 51$ K;[7] for *fac*-$[Mn^{II}(\mu\text{-}NC)_3(O_{tea})_2N_{tea}]$ (C.N. = 6) and $[Mn^{II}(\mu\text{-}CN)_4O_{tea}]$ (C.N. = 5, square pyramid) $T_C = 75$ K,[11] for *fac*-$[Mn^{II}(\mu\text{-}NC)_3(O_{tea})_2N_{tea}]$ (C.N. = 6) and $[Mn^{II}(\mu\text{-}CN)_4]$ (C.N. = 4, tetrahedron) $T_C = 106$ K) (tea = triethanoloamine).[11]

A natural extension of the studies of 3D magnetic octacyanometalate−Mn^{II} networks is investigation of the inorganic−organic hybrid assemblies built by $[Nb^{IV}(CN)_8]^{4-}$ and Mn^{II} building blocks. Although each Mn^{II} center has a potential to bridge up to six metal centers, in 3D $\{Mn^{II}_2(H_2O)_4[Nb^{IV}(CN)_8]\cdot 4H_2O\}$[38] coordinates four $[Nb^{IV}(CN)_8]^{4-}$ moieties. Use of organic linkers should give rise to a number of related, yet different, structural topologies derived from the same basic structural $Mn^{II}_2Nb^{IV}$ unit tuned by N- or/and O-donor organic linker. We presumed that organic linker will modify the metric parameters of Mn−NC−Nb linkages and introduce the additional coordination and magnetic arrangement in the form of organic $\{M-(\mu\text{-}L)\}_n^{2n+}$ or $\{M-L-M\}^{4+}$ open motives. We chose three organic linkers of well-documented ability to ensure the magnetic coupling between d-metallic connectors with the magnitude of J intermetallic coupling constants of one-tenth to units: pz,[44−54] pzdo[17,55] (pyrazine-*N*,*N*′-dioxide), and bpym.[33,56,57] The presence of the $\{M-(\mu\text{-}L)\}_n^{2n+}$ polymeric arrangement may influence magnetic ordering implying metamagnetic behavior or an increase of T_c values.[17,44−47,50−55]

Herein, we present three 3D high-T_c ferrimagnetic organic−inorganic hybrid materials with Mn^{II}−L−Mn^{II} and Mn^{II}−NC−Nb^{IV} linkages: $\{Mn^{II}_2(pz)_2(H_2O)_4[Nb^{IV}(CN)_8]\}\cdot pz\cdot 3H_2O$ (**1**), $\{Mn^{II}_2(pzdo)(H_2O)_4[Nb^{IV}(CN)_8]\}\cdot 5H_2O$ (**2**), and $\{Mn^{II}_2(bpym)(H_2O)_2[Nb^{IV}(CN)_8]\}$ (**3**). We describe and discuss the magneto-structural correlation of these novel compounds based on the spin-density properties provided by adequate heterobimetallic systems containing octacyano-

(33) Herrera, J. M.; Armentano, D.; de Munno, G.; Lloret, F.; Julve, M.; Verdaguer, M. *New J. Chem.* **2003**, *27*, 128−133.
(34) Kashigawi, T.; Ohkoshi, Sh.-ich.; Seino, H.; Mizobe, Y.; Hashimoto, K. *J. Am. Chem. Soc.* **2004**, *126*, 5024−5025.
(35) Korzeniak, T.; Stadnicka, K.; Rams, M.; Sieklucka, B. *Inorg. Chem.* **2004**, *43*, 4811−4813.
(36) Podgajny, R.; Bałanda, M.; Sikora, M.; Borowiec, M.; Spałek, L.; Kapusta, Cz.; Sieklucka, B. *Dalton Trans.* **2006**, 2801−2809.
(37) Eckhardt, R.; Hanika-Heidl, H.; Fischer, R. D. *Chem. Eur. J.* **2003**, *9*, 1795−1804.
(38) Pilkington, M., Decurtins, S. *Chimia* **2000**, *54*, 593−601.
(39) Pradhan, R.; Desplanches, C.; Guionneau, Ph.; Sutter, J.-P. *Inorg. Chem.* **2003**, *42*, 6607.
(40) Chibotaru, L. F.; Mironov, V. S.; Ceulemans, A. *Angew. Chem., Int. Ed.* **2001**, *40*, 4429−4433.
(41) Ruiz, E.; Rajaraman, G.; Alvarez, S.; Gillon, B.; Stride, J.; Clérac, R.; Larionova, J.; Descurtins, S. *Angew. Chem., Int. Ed.* **2005**, *44*, 2711−2715.
(42) Visinescu, D.; Desplanches, C.; Imaz, I.; Bahers, V.; Pradhan, R.; Villamena, F. A.; Guionneau, Ph.; Sutter, J.-P. *J. Am. Chem. Soc.* **2006**, *128*, 10202−10212.
(43) Clima, S.; Hendrickx, M. F. C.; Chibotaru, L. F.; Sonchini, A.; Mironov, V.; Ceulemans, A. *Inorg. Chem.* **2007**, *46*, 2682−2690.
(44) Manson, J. L.; Incarvito, Ch. D.; Rheingold, A. L.; Miller, J. S. *J. Chem. Soc., Dalton Trans.* **1998**, 3705−3706.
(45) Manson, J. L.; Huang, Q.-Zh.; Lynn, J. W.; Koo, H.-J.; Whangbo, M.-H.; Bateman, R.; Otsuka, T.; Wada, N.; Argyriou, D.; Miller, J. S. *J. Am. Chem. Soc.* **2001**, *123*, 162−172.
(46) Manson, J. L.; Arif, A. M.; Miller, J. S. *Chem. Commun.* **1999**, 1479−1480.
(47) Ishida, T.; Kawakami, T.; Mitsubori, Sh.-ich.; Nogami, T.; Yamaguchi, K.; Iwamura, H. *J. Chem. Soc., Dalton Trans.* **2002**, 3177−3186.
(48) Richardson, H. W.; Wasson, J. R.; Hatfield, W. E. *Inorg. Chem.* **1977**, *16*, 484−486.
(49) Haddad, M. S.; Hendrickson, D. N.; Cannady, J. P.; Drago, R. S.; Bieksza, D. S. *J. Am. Chem. Soc.* **1979**, *101*, 898−906.
(50) Real, J. A.; De Munno, G.; Muñoz, M. C.; Julve, M. *Inorg. Chem.* **1991**, *30*, 2701−2704.
(51) Hao, X.; Wei, Y.; Zhang, Sh. *Chem. Commun.* **2000**, 2271−2272.
(52) Lloret, F.; De Munno, G.; Julve, M.; Cano, J.; Ruiz, R.; Caneschi, A. *Angew. Chem., Int. Ed.* **1998**, *37*, 135−138.
(53) Otieno, T.; Rettig, St. J.; Thompson, R. C.; Trotter, J. *Inorg. Chem.* **1993**, *32*, 4384−4390.
(54) Woodward, F. M.; Gibson, P. J.; Jameson, G. B.; Landee, Ch. P.; Turnbull, M. M.; Willett, R. D. *Inorg. Chem.* **2007**, *46*, 4256−4266.
(55) Sun, H.-L.; Ma, B.-Q.; Gao, S.; Su, G. *Chem. Commun.* **2001**, 2586−2587.
(56) de Munno, G.; Ruiz, R.; Lloret, F.; Faus, J.; Sessoli, R.; Julve, M. *Inorg. Chem.* **1995**, *34*, 408−411.
(57) Armentano, D.; de Munno, G.; Guerra, F.; Faus, J.; Lloret, F.; Julve, M. *Dalton Trans.* **2003**, 4626−4634.

metalates. We prove that the magnitude of T_c is related to the number of cyano bridges per Mn_2Nb unit, the type of coordination polyhedra of $[Nb(CN)_8]^{4-}$, and coexistence of inorganic and organic connectivity. We also show that the FC/ZFC responses appear to be sensitive to the degree of organic connectivity.

Experimental Section

Materials. Pyrazine and bipyrimidine were purchased from commercial sources (Aldrich) and used without further purification. Potassium octacyanoniobate(IV) dihydrate $K_4[Nb(CN)_8]\cdot 2H_2O$[58] was prepared according to literature procedures. Pyrazine-*N*,*N*′-dioxide (pzdo) was synthesized according to modified literature methods (for details, see Supporting Information).[59,60]

Syntheses. *$\{Mn^{II}_2(pz)_2(H_2O)_4[Nb^{IV}(CN)_8]\}\cdot pz\cdot 3H_2O$ (**1**).* Dark yellow, rhombic single crystals of **1** were grown by slow diffusion of three substrate solutions in an H-shaped tube of total volume 8 mL during the period of 2 weeks. Aqueous solutions of the potassium octacyanoniobate(IV) (0.24 mmol, 120 mg, 0.5 mL) in one arm and manganese(II) chloride (0.5 mmol, 99 mg, 0.5 mL) in the other were connected with an aqueous solution of pyrazine (5.25 mmol, 420 mg, 7 mL). Product was washed with water and dried in air. Yield: ca. 20%. Anal. Calcd for $C_{20}H_{26}Mn_2N_{14}NbO_7$: C, 30.9; H, 3.4; N, 25.2. Found: C, 30.8; H, 3.5; N, 24.9. IR (in KBr, cm^{-1}): 2160 m(sh), 2141 vs, 2125 m(sh), 2098 w, 1639 s, 1616 s, 1489 vw, 1420 vs, 1350 vw, 1231 vw, 1156 m, 1126 m, 1109 w, 1079 m, 1052 m, 1043 m, 914 vw, 799 m, 469 m, 449 m, 441 m, 418 w(sh). **1** undergoes slow decomposition in ambient conditions. TGA/DTG/QMS measurements done on freshly prepared sample show three peaks in the temperature regions 40−90, 90−120, and above 120 °C assigned to the collective loss of H_2O (line $q/m = 18^+$), cyanide (lines $q/m = 26^+$ and 27^+, and pyrazine ($q/m = 80^+$). The two first regions are dominated by loss of crystallization and coordination H_2O, respectively, while the third one is dominated by loss CN^- and pz.

*$\{Mn^{II}_2(pzdo)(H_2O)_4[Nb^{IV}(CN)_8]\}\cdot 5H_2O$ (**2**).* Aqueous solutions of $MnCl_2\cdot 4H_2O$ (0.25 mmol, 49.5 mg, 5 mL) and pzdo (2 mmol, 224 mg, 10 mL) were mixed. Afterward an aqueous solution of $K_4[Nb(CN)_8]\cdot 2H_2O$ (0.25 mmol, 124 mg, 10 mL) was added. The resulting yellow solution was filtered and left to stand in the dark. After 24 h orange single crystals suitable for structure determination were obtained. Yield: 11%. Anal. Calcd for $C_{12}H_{22}Mn_2N_{10}NbO_{11}$: C, 21.0; H, 3.2; N, 20.4. Found: C, 21.4; H, 3.3; N, 20.3. IR (in KBr, cm^{-1}): 2153 m(sh), 2146 w(sh), 2141 w(sh), 2134 s, 1643 s, 1618 s, 1481 m, 1456 s, 1314 vw, 1289 w, 1248 m, 1233 m, 1190 w, 1090 w, 1056 m, 849 m, 811 s. **2** undergoes slow decomposition in ambient conditions. TGA/DTG/QMS measurements done on freshly prepared sample show two peaks in the temperature regions 30−120 and above 120 °C assigned to collective loss of H_2O and CN^-. The first region is dominated by loss of crystallization and coordination H_2O, while the second one is dominated by loss of CN^-.

*$\{Mn^{II}_2(bpym)(H_2O)_2[Nb^{IV}(CN)_8]\}$ (**3**).* Yellow, single crystals of **3** were grown by slow diffusion of three substrate solutions in an H-shaped tube of total volume 8 mL during the period of 3 weeks. An aqueous solution of the potassium octacyanoniobate(IV) (0.1 mmol, 50 mg in 0.5 mL) in one arm and an aqueous mixture of $MnCl_2\cdot 4H_2O$ (0.5 mmol, 99 mg, 0.75 mL) with bipyrimidine (0.5 mmol 80 mg in 0.75 mL) in the other were connected with an aqueous solution of bipyrimidine (0.42 g in 7 mL). Product was washed with water and dried in air. Yield: ca. 25%. Anal. Calcd for $C_{16}H_{10}Mn_2N_{12}NbO_2$: C 31.8; H 1.7; N 27.9. Found: C, 31.8; H, 1.8; N 27.5. IR (in KBr, cm^{-1}): 3477 vs, 3398 vs, 2162 s, 2127 vs, 1630 s, 1571 vs, 1411 vs, 1277 m, 1249 w, 1216 w, 1147 w, 1101 w, 1019 m, 829 m, 757 s, 690 m, 667 s, 585 m (br), 473 w(sh), 453 vs. **3** is stable in air. TGA/DTG/QMS measurements show no weight loss below 120 K; then collective decomposition starts.

Structure Solution and Refinement. The single-crystal diffraction data were collected on a Nonius Kappa CCD equipped with a Mo Kα radiation source and graphite monochromator. The space groups were determined using the ABSEN[61] program. For compounds **1** and **2** the structures were solved by the Patterson method using SHELXS-97.[62] The structure of compound **3** was solved by direct methods using SIR-97.[63] Refinement and further calculations for all compounds were carried out using SHELXL-97.[62] The non-H atoms were refined anisotropically using weighted full-matrix least-squares on F^2. All hydrogen atoms joined to carbon atoms in organic components of the discussed compounds were positioned with an idealized geometry and refined using a riding model with U_{iso}(H) fixed at $1.2U_{eq}$(C). All reachable H atoms in water molecules were found from the difference Fourier map and then refined using a riding model (AFIX 3) with U_{iso}(H) fixed at $1.5U_{eq}$(O). Selected crystallographic data for the studied compounds are shown in Table 2. Structural diagrams were prepared using Mercury 1.4.1 or ORTEP 32[64] software.

Physical Techniques. Infrared spectra were measured in KBr pellets between 4000 and 400 cm^{-1} using a Bruker EQUINOX 55 spectrometer. Elemental analyses were performed on a EuroEA EuroVector elemental analyzer. Thermogravimetric data in the temperature range 25−400 °C were collected on a Mettler Toledo TGA/SDTA 851e microgravimeter equipped with QMS Thermostar GSD 300 T Balzers at a heating rate of 5 °C/min in an Ar atmosphere. Magnetic susceptibility vs temperature, *T*, and vs magnetic field, *H*, was performed using a Quantum Design SQUID magnetometer.

Results

Synthetic Strategy. Compound **1** was prepared according to the two-step strategy[35,36] consisting of cross-linking the preorganized pyrazine-bridged $\{Mn^{II}-(\mu\text{-pz})\}_n^{2n+}$ chains by octacyanoniobate ions. Taking into account the influence of the reaction conditions on formation of possible homometallic Mn−pz byproducts[65] or heterometallic $\{Mn^{II}_2(H_2O)_4[Nb^{IV}(CN)_8]\cdot 4H_2O\}$ we used a large excess of pyrazine over Mn^{II} and $[Nb^{IV}(CN)_8]^{4-}$ ions in the H tube. Compound **2** was afforded in a one-pot reaction under using excess organic linker over metal ions with a molar ratio of pzdo:Mn of 8:1. The synthetic strategy for compound **3** was adapted from the literature method (slow diffusion in the H tube) applied

(58) Kiernan, P. M.; Griffith, W. P. *J. Chem Soc., Dalton Trans.* **1975**, 2489−2494.
(59) Simpson, G.; Vinciguerra, A.; Quagliano, J. V. *Inorg. Chem.* **1963**, *2*, 282−286.
(60) Klein, B.; Berkowitz, J. *J. Am. Chem. Soc.* **1959**, *81*, 5160−5166.
(61) McArdle, P. *J. Appl. Crystallogr.* **1996**, *29*, 306.
(62) Sheldrick, G.M. *SHELX97 [Includes SHELXS97, SHELXL97, CIFTAB (and SHELXA)], Programs for Crystal Structure Analysis* (Release 97−2); Institüt für Anorganische Chemie der Universität: Göttingen, Germany, 1998.
(63) SIR9. Altomare, A.; Burla, M. C.; Camalli, M.; Cascarano, G. L.; Giacovazzo, C.; Guagliardi, A.; Moliterni, A. G. G.; Polidori, G.; Spagna, R. *J. Appl. Crystallogr.* **1999**, *32*, 115−119.
(64) Farrugia, L. J. *J. Appl. Crystallogr.* **1997**, *30*, 565.
(65) Näthler, Ch.; Greve, J. *J. Solid State. Chem.* **2003**, *176*, 259−265.

Table 2. Experimental and Crystal Data for **1**−**3**

	1	**2**	**3**
empirical formula	$C_{80}H_{100}Mn_8N_{56}Nb_4O_{28}$	$C_{48}H_{96}Mn_8N_{40}Nb_4O_{52}$	$C_{16}H_{10}Mn_2N_{12}HbO_2$
fw (g·mol^{-1})	3104.52	2876.04	605.15
cryst syst	triclinic	monoclinic	mononoclinic
space group	*P*1	*C*2/*c*	*C*2/*c*
unit cell dimens	a = 10.947(5) Å b = 17.908(5) Å c = 19.308(5) Å α = 63.446(5)° β = 75.227(5)° γ = 73.788(5)°	a = 15.875(5) Å b = 15.061(5) Å c = 12.052(5) Å β = 108.215(5)°	a = 14.713(5) Å b = 12.731(5) Å c = 12.249(5) Å β = 103.298(5)°
V (Å^3)	3213.6(19)	2737.2(17)	2232.9(15)
Z	1	1	4
d_{calcd} (Mg·m^{-3})	1.604	1.745	1.800
T (K)	293(2)	293(2)	293(2)
abs coeff (mm^{-1})	1.185	1.394	1.659
F(000)	1559	1443	1188
wavelength (Å)	0.71069	0.71069	0.71069
cryst size (mm^3)	0.25 × 0.25 × 0.03	0.30 × 0.08 × 0.05	0.35 × 0.12 × 0.12
θ range for data collection (deg)	2.72−33.72	2.31−37.79	2.14−32.01
index ranges	$-16 \le h \le 17$ $-27 \le k \le 26$ $-27 \le l \le 30$	$-26 \le h \le 27$ $-23 \le k \le 25$ $-20 \le l \le 20$	$-19 \le h \le 21$ $-18 \le k \le 18$ $-15 \le l \le 18$
reflns coll	37 577	22 767	11 575
indep reflns	25 409 [R(int) = 0.0377]	7271 [R(int) = 0.0641]	3892 [R(int) = 0.0298]
completeness of θ (%)	99.1	99.0 (θ to 37.9°)	100.0 (θ to 32.01°)
max/min transmission	0.9653/0.7561	0.9336/0.6798	0.8258/0.5944
refinement method	full-matrix least-squares on F^2		
data/restraints/params	25409/3/803	7271/0/173	3892/3/158
weighting scheme	$w = 1/[\sigma^2(F_o^2) + (\alpha P)^2 + \beta P]$, where $P = (F_o^2 + 2F_c^2)/3$		
goodness-of-fit on F^2	1.047	1.046	1.102
final R indices [$I > 2\sigma(I)$]	R_1 = 0.0597 wR_2 = 0.0977	R_1 = 0.0477 wR_2 = 0.0915	R_1 = 0.0317 wR_2 = 0.0678
largest diff. peak and hole e·Å^{-3}	1.098 and −0.830	1.077 and −0.972	0.683 and −1.104

successfully in the case of $\{Mn^{II}_2(bpym)(H_2O)_2[M^{IV}(CN)_8]\}$ (M = Mo, W).[33]

Crystal Structures. The crystal structure of **1** is shown in Figures 1and 2 and Supporting Information Figures S1 and S2. The basic coordination units are linear 1D *trans*-$\{Mn^{II}-(\mu\text{-pz})\}_n^{2n+}$ chains interlocked with the 3D network of $Mn^{II}-CN-Nb^{IV}$ linkages into the hybrid organic−inorganic 3D coordination framework (Figures 1 and 2). The constitution is completed by monocoordinated and crystallization pyrazine as well as coordination and crystallization water molecules. Crystallization pyrazine molecules are stabilized by hydrogen bonding to H_2O molecules and strong $\pi-\pi$ interaction with two bridging pyrazine molecules (Figure S1). Selected details of the manganese and niobium coordination units are presented in Figure S2 and Table S1. Mn1, Mn2, and Mn3 centers forming $\{Mn^{II}-(\mu\text{-pz})\}_n^{2n+}$ chains coordinate two nitrogen atoms of bridging pyrazine, two nitrogen atoms of $[Nb(CN)_8]^{4-}$ moieties, and two oxygen atoms of aqua ligands in a *trans*-elongated octahedral geometry. Within the chain the dihedral angle between the plane of the bridging pz molecule and the $MnN_2(N_{pz})_2$ or

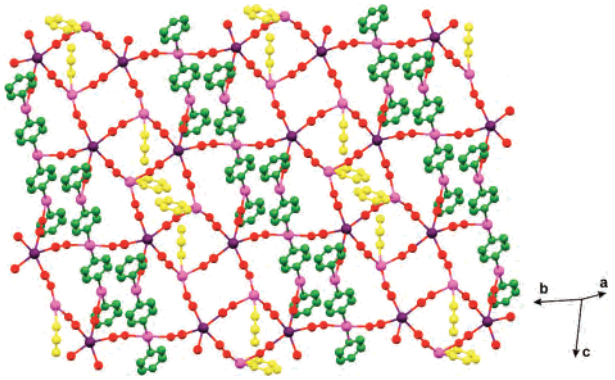

Figure 1. 2D view of the crystal structure of **1**: Nb (dark violet), Mn (light pink), bridging pyrazine (green), monodentate pyrazine (yellow), CN^- (red). Crystallization molecules of pyrazine and water molecules along with nonbridging CN^- are omitted for clarity.

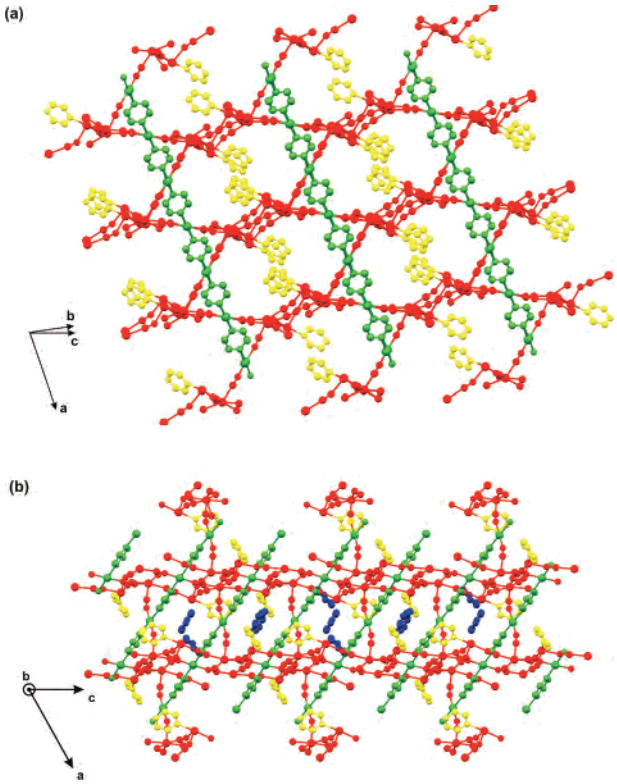

Figure 2. 3D packing diagram of **1**: (a) 1D $\{Mn-(\mu\text{-pz})\}_n^{2n+}$ chains (green) cross-linked with 3D cyano-bridged framework (red) including monocoordinated pz (yellow); (b) crystallization pz molecules (blue) trapped between neighboring $\{Mn-(\mu\text{-pz})\}_n^{2n+}$ chains by $\pi-\pi$ stacking interaction. Water molecules and terminal CN^- ligands are omitted for clarity.

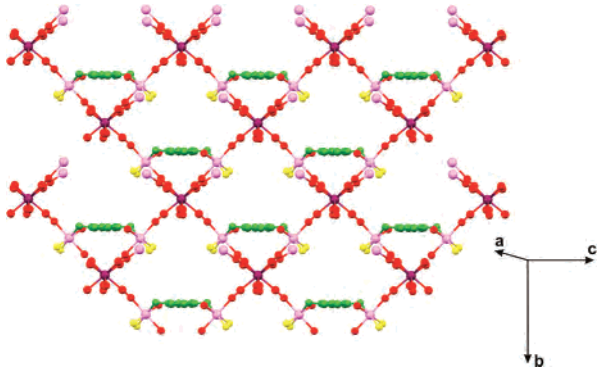

Figure 3. 2D fragment of crystal structure of **2**: 2D Mn_2Nb sheets of square grid topology: pzdo ligands in $[Mn^{II}_2-(\mu\text{-pzdo})]$ dimers (green), Nb (dark violet), Mn (light pink), CN^- (red), aqua ligands (yellow).

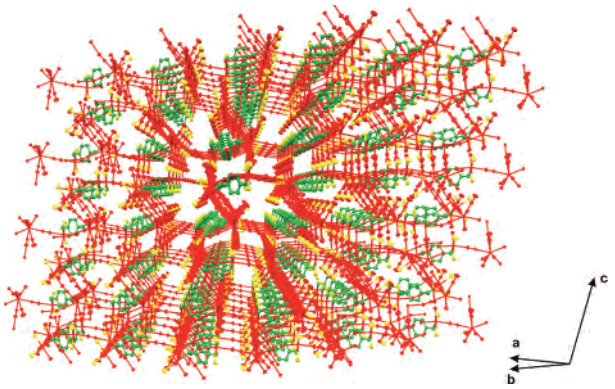

Figure 4. Packing diagram of **2**: pzdo ligands in $[Mn^{II}_2-(\mu\text{-pzdo})]$ dimers (green), extended 3D cyano-bridged network (red), aqua ligands (yellow).

$Mn(N_{pz})_2O_2$ plane of the Mn complex is very close to 45°. Mn4 and Mn5 centers are involved in a cyano-bridged network only. They coordinate three nitrogen atoms of the $[Nb(CN)_8]^{4-}$ units in a *fac*-geometry, two oxygen atoms of the aqua ligands, and one nitrogen atom of the monodentate pyrazine molecule. The geometry of Mn4 and Mn5 deviates strongly from an ideal octahedron. $[Nb(CN)_8]^{4-}$ moieties of square-antiprismatic (SAPR) geometry distorted toward dodecahedral (DD) coordinate five bridging and three terminal cyano ligands, giving rise to mixed Nb:Mn 5:2 and 5:3 inorganic connectivity. The metric parameters are in agreement with those of $[Nb(CN)_8]^{4-}$ moieties[38,39] and those of Mn−pyrazine coordination compounds.[44−46,65−67]

The crystal structure of **2** is shown in Figures 3and 4 and Supporting Information Figure S3. The extended 3D cyano-bridged coordination framework is built of waved 2D niobium-nodded Mn_2Nb sheets of square grid topology (Mn−N1−C1−Nb and Mn−N4−C4−Nb linkages) (Figure 3) joined together by a system of Mn−N3−C3−Nb linkages (Figure 4). The architecture of the 3D framework results in channels filled with bridging pzdo molecules as well as coordination and crystallization H_2O molecules involved in the hydrogen bonding and van der Waals interaction network. It may be also perceived as a supramolecular 3D coordination scaffold constructed of sets 1D straight NbMn ladders

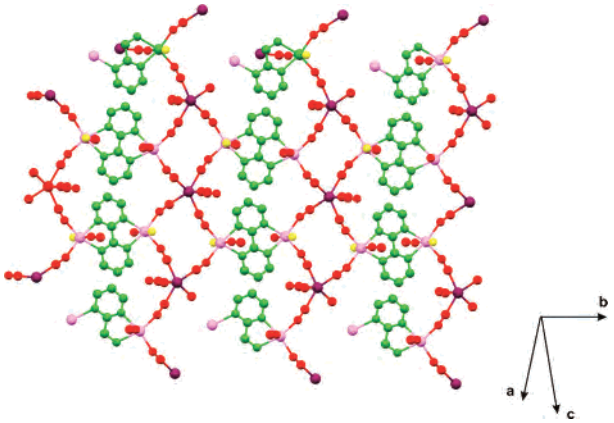

Figure 5. 2D fragment of the crystal structure of **3**: bpym in $[Mn^{II}_2-(\mu\text{-bym})]$ dimers (green), Nb (dark violet), Mn (light pink), CN^- (red), aqua ligands (yellow).

interlocked in Nb centers (Figure 4). The pzdo molecules create the dimeric coordination arrangement, forming pzdo-capped $[Mn^{II}_2-(\mu\text{-pzdo})]-\{(\mu\text{-CN})_2-[Nb^{IV}(CN)_6]\}$ triangles (Figure S3). The most important metric parameters are presented in Table S1. Manganese centers coordinate three nitrogen atoms $[Nb(CN)_8]^{4-}$ units in the *mer*-geometry. The pseudo-octahedral coordination is completed by two oxygen atoms of H_2O ligands molecules and one oxygen end of the pzdo ligand bridging Mn(II) centers of Mn_2(pzdo)Nb triangles. The bridging coordination of pzdo is realized by the almost ideal gauche conformation with a torsion angle Mn−O−O′−Mn′ of 91.7°.[68] The observed conformation is different from the trans one observed for homometallic Mn(NCS)$_2$(pzdo)$_2$[55] and MnN_3pzdo[17] as well as $[Mn(NCS)_2(2,5\text{-dmpdo})_{1.5}(H_2O)_2]\cdot 0.5(2,5\text{-dmpdo})\cdot H_2O$, $Mn(N_3)_2(2,5\text{-dmpdo})(H_2O)_2$, and Mn(dca)$_2$(2,5-dmpdo) (2,5-dmpdo = 2,5-dimethylopyridine-*N*,*N*′-oxide, dca^- = dicyanamid) networks (Mn−O−O′−Mn′ angle = 180°).[69] The basal plane of the pzdo ligands is oriented parallel to the square planes of $[Nb(CN)_8]^{4-}$ with close contact distances $C_{pzdo}\cdots N_{CN}$ and $O_{pzdo}\cdots N_{CN}$ of about 3 Å. Octacyanoniobate moieties have intermediate geometry between square antiprism and dodecahedron (DD) and coordinate six neighboring manganese centers, giving rise to Nb:Mn 6:3 inorganic connectivity. The metric parameters are in agreement with those of $[Nb(CN)_8]^{4-}$ moieties.

The crystal structure of **3** is shown in Figures 5 and 6 and Supporting Information Figure S4. The basic coordination units are dimeric $\{Mn_2(\mu\text{-bpym})\}^{2+}$ moieties exhibiting a bis-chelating coordination mode of bpym (Figure S4). Coordination of octacyanoniobate(IV) (Mn−N1−C1−Nb and Mn−N4−C4−Nb linkages) leads to 2D layers built of alternatively aligned stripes of $\{Mn_2(\mu\text{-bpym})\}^{2+}$ and Nb_2Mn_2 squares involved in cyano-bridged ribbons (Figure 5). Further coordination of $[Nb(CN)_8]^{4-}$ (Mn−N3−C3−Nb linkage) leads to a closely packed 3D cyano-bridged network (Figure 6). The constitution is completed by coordinated H_2O molecules. No crystallization molecules are observed. The

(66) Kumagai, H.; Kawata, S.; Kitagawa, S. *Inorg. Chim. Acta* **2002**, *337*, 387−392.
(67) Ma, Ch.; Wang, W.; Zhang, X.; Chen, Ch.; Liu, Q.; Zhu, H.; Liao, D.; Li, L. *Eur. J. Inorg. Chem.* **2004**, 3522−3532.
(68) Sun, H.-L.; Gao, S.; Ma, B.-Q.; Chang, F.; Fu, W.-F. *Mic. Mes. Mater.* **2004**, *73*, 89−95.
(69) Sun, H.-L.; Gao, S.; Ma, B.-Q.; Su, G.; Batten, St. R. *Cryst. Growth Des.* **2005**, *5*, 269−277.

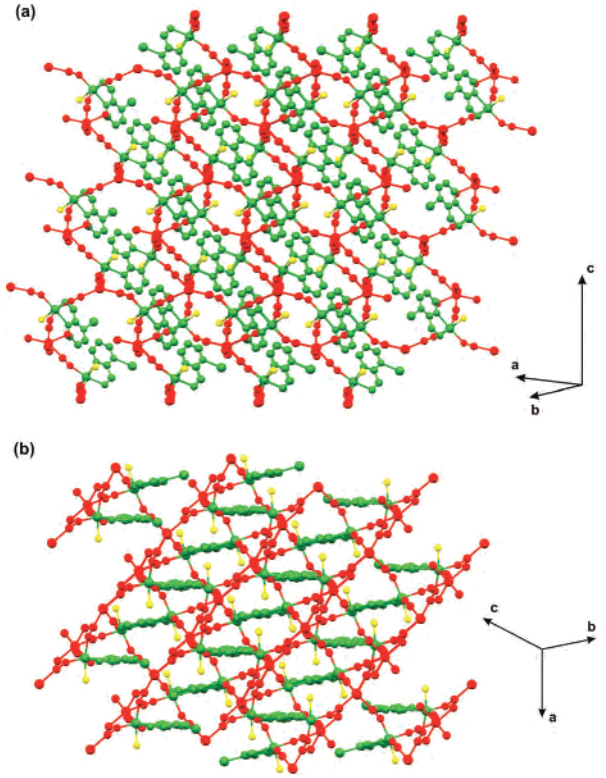

Figure 6. Packing diagrams of **3** showing 3D inorganic connectivity of cyano-bridged network (red) and organic connectivity Mn centers linked with μ-bpym ligand into {Mn_2(μ-bpym)} dimeric subunits (green) and aqua ligands (yellow).

Table 3. Deconvoluted IR Spectra of **1**−**3** in the ν(CN) Region[a]

$K_4[Nb(CN)_8]\cdot 2H_2O$		**1**	**2**	**3**
	2112 w[c]	2098 vw	2134 vs	2126 m
2114 vs[b]	2114 s[c]	2123 m	2141 w	2141 w
2123 s[b]	2125 m[c]	2141 s	2146 m	2162 m
2129 s[b]	2131 m[c]	2157 m	2153 s	
2136 s[b]	2138 m[c]			

[a] The frequencies (in cm^{-1}) of $K_4[Nb(CN)_8]\cdot 2H_2O$ are used as a reference. [b] Reference 58. [c] This work.

most important metric parameters are presented in Table S1. Manganese centers coordinate three nitrogen atoms $[Nb(CN)_8]^{4-}$ units in *fac*-geometry. Pseudo-octahedral coordination is completed by one oxygen atom of H_2O molecules and two chelating nitrogen atoms bridging the bpym ligand. Octacyanotungstate moieties of almost ideal dodecahedral (DD) geometry coordinate six neighboring manganese centers, giving rise to Nb:Mn 6:3 inorganic connectivity. **3** is isomorphic to the {μ-(bpym)[$Mn^{II}(H_2O)$]$_2$-μ-$(NC)_6M^{IV}(CN)_2$} (M = Mo, W) networks reported recently.[33]

IR Spectroscopy. The signatures of C≡N stretching modes render infrared spectroscopy a useful tool for characterization of octacyanometalates based coordination networks. The IR spectra of **1**−**3** in the ν(CN) region together with their Gaussian deconvolution as well as spectra of $K_4[Nb(CN)_8]\cdot 2H_2O$ are presented in Figures S5 and Table 3. The spectra exhibit strong broad complex absorption bands in 2090−2180, 2110−2170, and 2100−2170 cm^{-1} wavenumber range, respectively. Comparison to the spectra of ionic potassium salts of $[Nb(CN)_8]^{4-}$[58] shows additional bands above 2140 cm^{-1}, which are generally assignable to bridging modes of CN^- ligands.[70] The compounds do not exhibit any regular dependence between the bridging-to-terminal CN^- ligands ratio and the intensity ratio of appropriate bands. We interpret the whole ν(CN) region of **1**−**3** to be intrinsic features related to the σ- and π-donor as well as π-acceptor properties of bridging cyanides of respective networks.[71]

Spectra of **1** and **2** along with spectra of relevant linker in the solid state in the range characteristic for vibrations of organic molecules are presented in Figures S6 and S7, respectively. The spectrum of **1** exhibits significant changes compared to the spectrum of free pyrazine (Figure S6).[72] The 469, 449, and 441 cm^{-1} bands are representative for the $[Nb(CN)_8]^{4-}$ moiety (skeletal ν(Nb−C))[58] as well as coordinated pyrazine,[73−77] while the very visible shoulder at ca. 417 cm^{-1} is attributed to a crystallization molecule of pyrazine.[72] The changes in the energy and intensity are also seen in the 1200−1000 cm^{-1} region characteristic of γ(ArCH in-plane) vibrations, and we attribute them to the presence of bridging, monocoordinated, and hydrogen-bond- and π−π stacking-stabilized pyrazine.

The spectrum of **2** exhibits significant changes compared to the spectrum of free pzdo (Figure S7).[60] The changes are attributed to the presence of bridging modes of pzdo. The most pronounced shifts are seen in the 850−880, 1030−1060, and 1230−1280 cm^{-1} regions.

The spectrum of **3** in the range 1800−400 cm^{-1} (Figure S8) generally exhibits features characteristic for coordinated bpym ligand including the presence of a very strong band at 1580 cm^{-1} along with the absence of a band close to 1530 cm^{-1}, both characteristic of bis-chelation of the bpym ligand.[33]

Magnetic Properties. The temperature dependences of the magnetic susceptibility $M(T)$ measured at 1 kOe for magnetic networks **1**−**3** are presented in Figure 7. The high-temperature χT product values of 8.8 (**1**), 8.9 (**2**), and 8.6 (**4**) $cm^3\cdot mol^{-1}\cdot K$ are very close to 9.13 $cm^3\cdot mol^{-1}\cdot K$ expected for two high-spin Mn^{II} (S = 5/2) and one Nb^{IV} (S = 1/2) assuming g = 2.0. On cooling M values increase slowly; then the signals increase, abruptly reaching the highest point at about 27 (**1**), 37 (**2**), and 50 (**3**) K, then saturating at low temperatures. Such a temperature dependence of M suggests the presence of long-range magnetic ordering below critical temperatures T_c. The $M(H)$ dependences of **1**−**3**, measured at 2 K, are presented in the Figure 7. The values of

(70) Podgajny, R.; Korzeniak, T.; Stadnicka, K.; Dromzée, Y.; Alcock, N. W.; Errigton, W.; Kruczała, K.; Bałanda, M.; Kemp, T. J.; Verdaguer, M.; Sieklucka, B. *Dalton Trans.* **2003** 3458−3468.
(71) Kettle, S. F. A.; Diana, E.; Boccaleri, E.; Stanghellini, P. L. *Inorg. Chem.* **2007**, *46*, 2409−2416.
(72) Lord, R. C.; Marston, A. L.; Miller, F. A. *Spectrochim. Acta* **1957**, *9*, 113.
(73) Goldstein, M.; Unsworth, W. D. *Spectrochim. Acta* **1971**, *27A*, 1055.
(74) Ferraro, J. R.; Zipper, J.; Wozniak, W. *Appl. Spectrosc.* **1969**, *23*, 160.
(75) Goldstein, M.; Taylor, F. B.; Unsworth, W. D. *J. Chem. Soc., Dalton Trans.* **1972**, 418.
(76) Haynes, J. S.; Sams, J. R.; Thompson, R. C. *Inorg. Chem.* **1986**, *25*, 3740.
(77) Haynes, J. S.; Kostikas, A.; Sams, J. R.; Simopoulos, A.; Thompson, R. C. *Inorg. Chem.* **1987**, *26*, 2630.

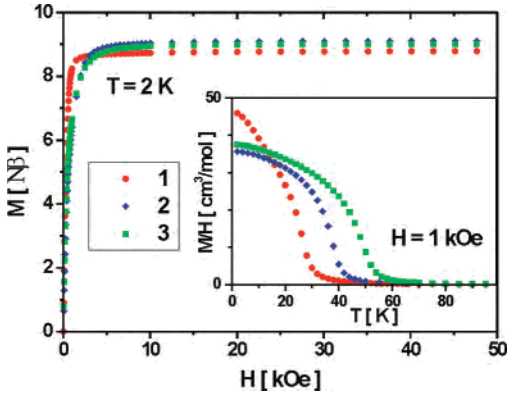

Figure 7. Magnetization per Mn_2Nb unit of **1** (red), **2** (blue), and **3** (green) measured at $T = 2$ K. (Inset) Temperature dependence of magnetization measured during cooling in $H = 1$ kOe.

magnetization at saturation M_{sat} are 8.8 (**1**), 9.1 (**2**), and 9.0 Nβ (**3**), strongly suggesting a magnetic structure with one Nb ($S = 1/2$) spin-up and two Mn ($S = 5/2$) spin-down, where a saturation value of 9 Nβ is expected. The increase of $M(H)$ signals is extremely fast, reaching about 95% of M_{sat} below $H = 2$ kOe. No magnetic hysteresis is observed at 2 K. The zero-field-cooled (ZFC) and field-cooled (FC) magnetizations, recorded at a magnetic field of 5 Oe, demonstrate sharp anomalies at 27 (**1**), 37 (**2**), and 50 K (**3**) (Figure S9), confirming magnetic ordering at these temperatures. All observations point out that **1**−**3** are soft, classical 3D ferrimagnets. The FC curve for **1** reveals the unusual behavior below 25 K along with the additional anomaly around 5 K, suggesting that magnetic structure undergoes further transitions, at least in low magnetic fields. The $\chi^{-1}(T)$ curves above ordering temperatures reveal two distinguishable regions of linearity with a slight shoulder around 90 (**1**), 150 (**2**), and 180 (**3**) K (Figure S10). Fitting the Curie−Weiss law $\chi^{-1} = (T - \theta_{CW})/C$ to the data above 100 for **1** and above 200 K for **2** and **3** gives $\theta_{CW} = 23$ (**1**), 7 (**2**), and 26 K (**3**) (in the case of **1** the fit is in the 100−150 K range).[78] In all three cases θ_{CW} values are significantly lower than ordering temperatures T_C, which is in agreement with the ferrimagnetic structure.

Discussion

X-ray structural characterization shows that the dominating bridging motifs responsible for the 3D coordination architecture in **1**−**3** are Nb^{IV}−CN−Mn^{II} linkages. We assign the presence of ordering temperature T_C in **1**−**3** mainly to the effective antiferromagnetic Nb(IV)−Mn(II) coupling through extended inorganic connectivity of the cyano-bridged framework. The magneto-structural correlation for 3D Mn_2Nb assemblies is presented in Table 4. The tentative geometry of the $[Nb(CN)_8]^{4-}$ moiety coordination polyhedra was proposed based on the detailed investigation of selected sets of dihedral angles between the normals of adjacent triangles, defined as δ, and nonplanarity of the trapezoidal-type atoms, defined by the angle ϕ (Table 5).[42,79] Precise determination of the structure of $[Nb(CN)_8]$ in **1**−**3** was performed using continuous shape measure (CShM) analysis for eight-coordinate polyhedra (Table 6).[80−84] Figure 8 presents the coordination environment of $[Nb(CN)_8]^{4-}$ moieties in **1**−**3**. In **1** $[Nb(CN)_8]^{4-}$ complexes with a geometry close to SAPR with the shape measures $S_{SAPR} = 0.47$ and 0.54 and $S_{DD} = 1.50$ and 1.66. $[Nb(CN)_8]^{4-}$ ions coordinate five Mn(II) centers (Figure 8a). In **2** octacyanoniobates(IV) have a geometry of intermediate character between SAPR and DD ($S_{SAPR} = 1.17$, $S_{DD} = 0.69$) and coordinate six Mn(II) complexes using six cyanides, four of them located at "vertexes B"-like and the remaining two located at "vertexes A"-like positions (Figure 8b). In **3** $[Nb(CN)_8]^{4-}$ has DD geometry ($S_{SAPR} = 2.33$, $S_{DD} = 0.28$) and coordinate six Mn(II) complexes using six cyanides, four of them located in the vertexes B and the remaining two vertexes A (Figure 8c). The relatively small values of parameter $\Delta_{(SAPR,DD)}$ indicate that the actual shapes of $[Nb(CN)_8]$ polyhedra in **1**−**3** are very close to the ideal SAPR → DD interconversion pathway, which makes the bicapped trigonal prism (BTP) contribution to be of minor importance. We correlate the observed increase of T_C from **1** (27 K) to **2** (37 K) and **3** (50 K) mainly with the change in the geometry of $[Nb(CN)_8]^{4-}$ coordination polyhedra from SAPR (**1**) via intermediate SAPR/DD (**2**) toward DD (**3**) and with the increase of the number of cyano bridges per each Nb center (**1** and **2**). We also denote the shorter and more bent Nb−CN−Mn linkages in higher T_C **3** compared to lower T_C **2**. A strong dependence of the magnitude and sign of the J coupling constant on the bending angle M′−NC−M″ linkages (M′, M″ = 3d-electronic metal ions) was observed for hexacyanometalate-based cyano-bridged assemblies.[85,86] This correlation in the case of octacyanometalates-based compounds may be, however, of minor significance as it was suggested by Ruiz et al. for Mo_6Mn_9 high-spin cluster.[41] Particularly interesting is the coincidence of T_C values (50 K) for **3** and the 3D ferrimagnetic $\{Mn^{II}_2(H_2O)_4[Nb^{IV}(CN)_8]\cdot 4H_2O\}$ network characterized by dominating SAPR character of $[Nb^{IV}(CN)_8]^{4-}$ and increased Nb:Mn inorganic connectivity (8:4) compared to **3** (6:3).[38] We relate this equality to the DD character of $[Nb^{IV}(CN)_8]^{4-}$ along with the four equatorial and two apical cyano bridges in **3**. This configuration may possibly ensure the spin density localized on CN^- bridges to be high enough

(78) The data were carefully corrected for background diamagnetism. Sample **1** seems to alter while being pumped out at room temperature, so the measurements were performed only below 150 K.

(79) Mueterties, E. L.; Guggenberger, L. *J. Am. Chem. Soc.* **1974**, *96*, 1748−1756.
(80) Casanova, D.; Cicera, J.; Llunell, M.; Alemany, P.; Avnir, D.; Alvarez, S. *J. Am. Chem. Soc.* **2004**, *126*, 1755−1763.
(81) Alvarez, S.; Alemany, P.; Casanova, D.; Cicera, J.; Llunell, M.; Avnir, D. *Coord. Chem. Rev.* **2005**, *249*, 1693−1708.
(82) Casanova, D.; Llunell, M.; Alemany, P.; Alvarez, S. *Chem. Eur. J.* **2005**, *11*, 1479−1494.
(83) Cicera, J.; Ruiz, E.; Alvarez, S. *Chem. Eur. J.* **2006**, *12*, 3162−3167.
(84) Llunell, M.; Casanova, D.; Cicera, J.; Bofill, J.M.; Alemany, P.; Alvarez, S.; Pinsky, M.; Avnir, D. *SHAPE v. 1.1b. Program for the Calculation of Continuous Shape Measures of Polygonal and Polyhedral Molecular Fragments*; University of Barcelona: Barcelona, Spain, 2005.
(85) Toma, L.; Toma, L. M.; Lescouëzec, R.; Armentano, D.; De Munno, G.; Andruh, M.; Cano, J.; Lloret, F.; Julve, M. *Dalton Trans.* **2005**, 1357.
(86) Zhang, Y.-Zh.; Gao, S.; Wang, Zh.-M.; Su, G.; Sun, H.-L.; Pan, F. *Inorg. Chem.* **2005**, *44*, 4534−4545.

Table 4. Magneto-structural Correlation for Networks Built by Octacyanoniobate(IV) and Manganese(II)

	1D chain $[Mn^{II}L]_2Nb^{IV}$ [h]	**1**	**2**	**3**	3D $Mn^{II}{}_2Nb^{IV}$ [i]
μ-inorg[a]	1	3	3	3	3
μ-org[b]		1	0	0	
Mn^{II} geometry	*trans*-(μ-NC)$_2$ pentagonal bipyramid	*trans*-(μ-NC)$_2$-*trans*-(μ-pyz)$_2$ elongated O_h, *fac*-(μ-NC)$_3$ pseudo-O_h	*mer*-(μ-NC)$_3$(μ-pzdo) pseudo-O_h	*fac*-(μ-NC)$_3$ pseudo-O_h	planar (μ-NC)$_4$ O_h
Mn−NC−Nb[c]	2 or 1	3 or 2	3	3	4
Nb^{IV} geometry	SAPR	SAPR (2×)[j]	Intermediate SAPR/DD[j]	DD[j]	SAPR
Nb−CN−Mn[d]	3	5	6 (4 equatorial + 2 apical)	6(4 equatorial + 2 apical)	8
T_C	2	27	37	50	50
Mn···Nb[e]	5.437(86)	5.501(90)	5.604(8)	5.448(56)	5.45
Mn−N−C[f]	148.,7	164.4	169.4	159.1	158
$Mn-N_{CN}$[g]	2.250(18)	2.189(14)	2.231(32)	2.174(27)	2.23

[a] Dimensionality of inorganic "μ-inorg" connectivity through the cyano bridges. [b] Dimensionality of organic "μ-org" connectivity through the pz (**1**), pzdo (**2**), and bpym (**3**) bridges. [c] Number of CN^- bridges per manganese(II) ion. [d] Number of CN^- bridges per niobium(IV) ion. [e] Average distance [Å]. [f] Average angle [deg]. [g] Average distance [Å]. [h] Reference 39. [i] Reference 38. L′ = macrocyclic ligand. [j] Type of polyhedra determined by analysis of δ and ϕ angles in $[Nb(CN)_8]$ polyhedra[42,79] and the continuous shape measure method[42,80−83] (see Tables 5 and 6, respectively).

Table 5. δ and ϕ Angles (deg) for Model and Experimental Eight-Vertex Geometries[42,79]

geometry	δ	ϕ
SAPR	0.0, 0.0, 52.4, 52.4	24.5
BTP	0.0, 21.8, 48.2, 48.2	14.1
DD	29.5, 29.5, 29.5, 29.5	0.0
$[Nb(CN)_8]$ in **1**	9.0, 16.0, 48.4, 46.9	21.1, 23.8
	6.0, 16.1, 51.5, 44.0	20.3, 19.3
$[Nb(CN)_8]$ in **2**	16.2, 24.8, 42.1, 42.1	11.2
$[Nb(CN)_8]$ in **3**	22.3, 34.0, 35.2, 35.2	3.7

Table 6. Continuous Shape Analysis[a] of the Coordination Sphere of the $[Nb(CN)_8]^{4-}$ Moiety in **1**−**3**

geometry	S_{SAPR}	S_{DD}	$\Delta_{(SAPR,DD)}$	$\varphi_{(SAPR\rightarrow DD)}$	$\varphi_{(DD\rightarrow SAPR)}$
SAPR	0.0	ca. 3.0	0.0	0%	100%
DD	ca. 3.0	0.0	0.0	100%	0%
$[Nb1(CN)_8]$ in **1**	0.47176	1.49723	0.13	40%	72%
$[Nb2(CN)_8]$ in **1**	0.54414	1.65866	0.20	44%	76%
$[Nb(CN)_8]$ in **2**	1.16643	0.69436	0.13	64%	49%
$[Nb(CN)_8]$ in **3**	2.32798	0.28069	0.22	90%	31%

[a] S_{SAPR} = the shape measure relative to the square antiprism; S_{DD} = the shape measure relative to the dodecahedron, $\Delta_{(SAPR,DD)}$ represents the deviation from the DD ↔ SAPR interconversion path; generalized interconversion coordinates $\varphi_{(SAPR\rightarrow DD)}$ and $\varphi_{(DD\rightarrow SAPR)}$ illustrate the change of dominating character of $[Nb(CN)_8]$ polyhedra on going from **1** to **3** (the sum $\varphi_{(SAPR\rightarrow DD)} + \varphi_{(DD\rightarrow SAPR)}$ is greater than 100% due to the nonzero value of $\Delta_{(SAPR,DD)}$). Data for ideal SAPR and DD taken from the SAPR-DD shape maps.[42,80−83]

to compensate for the difference in Nb:Mn connectivity of these two networks. Figures 9 and S11 represent the Mn(II)−NC−Nb(IV) magnetic coupling in networks **1**−**3**, qualitatively depicting the differences in overlap of π*(CN) orbitals with Nb magnetic orbitals $d_{x^2-y^2}$ (A vertex cyano bridge) (**3**) (Figure 9a), d_{z^2} (Figure 9b) (**1**), and d_{xv-y^2} (B vertex cyano bridge) (Figure 9c) (**3**). The extent of overlap is in agreement with the general trend of increasing spin density on going from the A vertex CN^- of DD via SAPR vertex CN^- toward B vertex in CN^- of DD found for $[Mo(CN)_8]^{3-}$ and $[W(CN)_8]^{3-}$ moieties.[42] All manganese(II) centers in **1**−**3** have a pseudo-octahedral environment ($t_{2g}{}^3e_g{}^2$ ground-state configuration) and effectively provide one-electron d_{xy}, d_{xz}, and d_{yz} orbitals, ensuring domination of antiferromagnetic coupling characteristic for cyano-bridged d^1 octacyanometalate−Mn(II) compounds ($M(d^1)$ = Nb^{IV}, Mo^V, and W^V).[38,41,87,88]

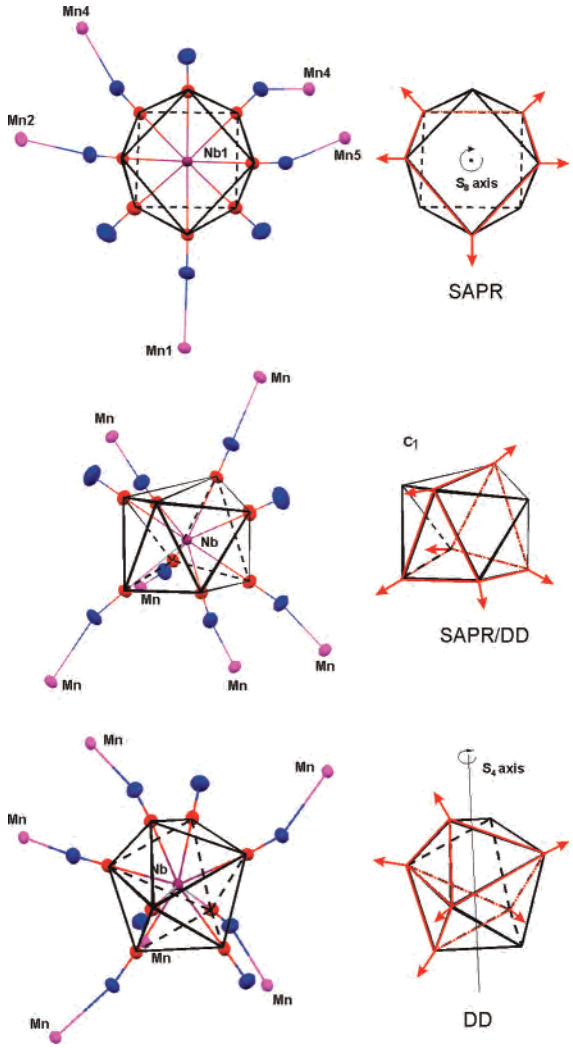

Figure 8. Coordination polyhedra and connectivity of $[Nb^{IV}(CN)_8]^{4-}$ inorganic linker in **1** (SAPR), **2** (intermediate between SAPR and DD), and **3** (DD): Nb (dark violet), C (red), N (blue), Mn (pink). Red arrows illustrate the direction of Nb−CN−Mn linkages.

The influence of organic linker on the magnetic signals of **1**−**3** relies strongly on the degree of organic connectivity. The unusual shape of FC−ZFC curves for **1** below T_C may be attributed to the presence of an additional organic

(87) Zhao, H.; Shatruk, M.; Prosvirin, A. V.; Dunbar, K. R. *Chem. Eur. J.* **2007**, DOI: 10.1002/chem.200700298.

(88) Przychodzen, P.; Korzeniak, T.; Podgajny, R.; Sieklucka, B. *Coord. Chem. Rev.* **2006**, *250*, 2234−2260.

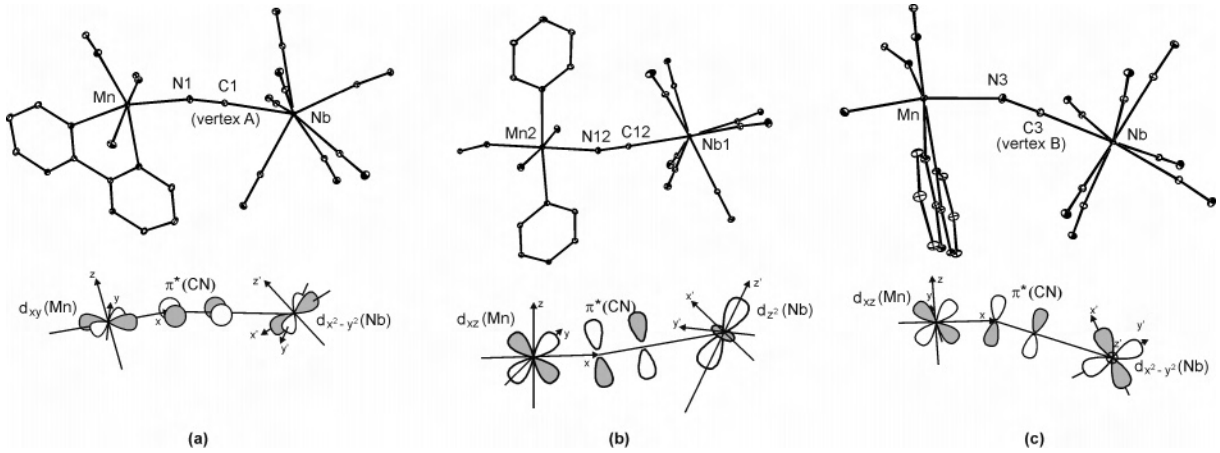

Figure 9. Overlap of Nb magnetic orbitals: (a) d_{x2-y2} at A vertex cyano bridge in **3** and (b) d_{z2} in **1** and (c) d_{x2-y2} in **3** at B vertex cyano bridge through π^*(CN) orbitals with the appropriate Mn manganese orbitals. In the case of **2** a, b, and c illustrate SAPR/DD intermediate character of the $[Nb(CN)_8]$ moiety.

sublattice represented by the $\{Mn^{II}-(\mu\text{-pz})\}_n^{2n+}$ 1D chains. 1D coordination of pz and 3d metal ions M^{II} (Mn^{II}, Co^{II}, Fe^{II}, Cu^{II}) is characterized by antiferromagnetic $M^{II}-pz-M^{II}$ interaction with the coupling constant $|J|$ of one-tenth to several cm^{-1} and in many cases strongly influences the magnetic ordering, implying metamagnetic behavior or the increase of T_c values.[44−47,50−54] The $|J_{MnMn}|$ values through the pz bridge are generally lower[44−47] than $|J_{MMn}|$ values for $Mn^{II}-NC-M^{V}(CN)_7$ (M = Mo, W) linkages, estimated to fall within the range from −3 to −23 cm^{-1}.[32,41,87,89] The cross-linking the $\{Mn^{II}-(\mu\text{-pz})\}_n^{2n+}$ 1D chains with a 3D cyano-bridged framework leads to competition between the antiferromagnetic interaction via $Mn^{II}-NC-Nb^{IV}$ and $Mn^{II}-pz-Mn^{II}$ linkages. Assemblies **2** and **3** are characterized by the local linking within dimeric entities only. The respective FC−ZFC curves reveal a shape characteristic of classical ferrimagnets without any additional features below T_C, which is correlated with the absence of any influence of organic connectivity. This observation is also in a good agreement with the negligibly small $|J_{MnMn}|$ coupling constant assumed for $\{Mn_2-(\mu\text{-pzdo})\}$ dimer in **2** and $|J_{MnMn}|$ calculated for $\{Mn_2-(\mu\text{-bpym})\}$ dimers ($J = -1.1$ cm^{-1})[33] in $\{Mn^{II}_2(bpym)(H_2O)_2[Nb^{IV}(CN)_8]\}$ (M = Mo, W) networks compared to the magnitude of $|J_{MMn}|$ values for $Mn^{II}-NC-M^{V}(CN)_7$ (M = Mo, W) linkages.

Conclusions

Our investigations on $Mn^{II}_2Nb^{IV}$ organic−inorganic hybrid networks have afforded a series of 3D cyano-bridged ferrimagnetic assemblies exhibiting long-range ordering below T_C in the range 27−50 K. Magneto-structural correlation reveals that the magnetic response depends on the structural parameters of **1**−**3**. The observed increase of T_C on going from **1** (27 K) to **2** (37 K) and **3** (50 K) is correlated with the approximate geometry of the $[Nb(CN)_8]^{4-}$ moiety, SAPR for **1**, intermediate SAPR/DD for **2**, and DD for **3**, and to the increased number of cyano bridges per Mn_2Nb unit. Furthermore, the FC/ZFC characteristics are sensitive to the degree of coexisting organic connectivity related to $Mn^{II}-L-Mn^{II}$ linkages (L = pyrazine, pyrazine-*N*,*N*′-dioxide, and 2,2′-bipyrimidine). The pseudo-octahedral environment of Mn^{II} centers is of minor significance in the explanation of magnetic properties.

Complex $\{Mn^{II}_2(pz)_2(H_2O)_4[Nb^{IV}(CN)_8]\}\cdot pz\cdot 3H_2O$ (**1**) is the first example of a hybrid network that displays the coexistence of a cross-linked 3D cyano-bridged framework and 1D $\{M^{II}\text{-}(\mu\text{-L})\}_n^{2n+}$ chains, filling for the first time an empty space in the classification table of hybrid materials proposed by Cheetham et al. with a notation of I^3O^1.[27]

This research clearly indicates that this class of octacyanoniobate(IV) polynuclear hybrid materials has great potential as high T_c magnetic material that is worthy of further exploration. Studies in this field are in progress.

Acknowledgment. The study has been partially supported by the EC within its NoE project MAGMANet, contract no. NMP-3-CT-2005-515767.

Supporting Information Available: Crystallographic information (in CIF format) for **1**−**3**; ORTEP plots together with the accompanying bond lengths and angles for **1**−**3**; examples of supramolecular organization for **1**; IR spectra for **1**−**3**; FC/ZFC and $1/\chi(T)$ characteristics for **1**−**3**; schematic representation of orbitals mediating Mn−NC−Nb magnetic interaction. This material is available free of charge via the Internet at http://pubs.acs.org.

IC7018132

(89) Podgajny, R.; Desplanches, C.; Sieklucka, B.; Sessoli, R.; Villar, V.; Paulsen, C.; Wernsdorfer, W.; Dromzée, Y.; Verdaguer, M. *Inorg. Chem.* **2002**, *41*, 1323−1327.